Colloids and Surfaces A: Physicochem. Eng. Aspects 520 (2017) 817–825

Contents lists available at ScienceDirect

Colloids and Surfaces A: Physicochemical and Engineering Aspects

journal homepage: www.elsevier.com/locate/colsurfa

Surface and interface properties of benzethonium chloride-montmorillonite

S. Türker[a], F. Yarza[b], R.M.Torres Sánchez[b], S. Yapar[a,*]

[a] Ege University, Engineering Faculty Chemical Engineering Department, 35100 Bornova, İzmir, Turkey
[b] Technology Center of Mineral Resources and Ceramics (CETMIC) CONICET-CCT La Plata –CICBA, Camino Centenario y 506, (1897) M. B. Gonnet, Argentina

HIGHLIGHTS

- Organoclays from Montmorillonite (Mt) and Benzethonium Chloride (BZT), were prepared by using conventional and microwave heating methods.
- No evidence of changes in the arrangements of BZT, generated by the two intercalation methods studied, were found by XRD analysis, however a more crystalline of structure seems to be attained by traditional method.
- The adsorption kinetics fitted to pseudo second order kinetic model for BTZ amounts of 80% and 100% CEC.
- The basal spacing of the clay increased up to 2.85 nm with increasing amount of BTZ and a pseudo trimolecular layer formed in the interlayer.

GRAPHICAL ABSTRACT

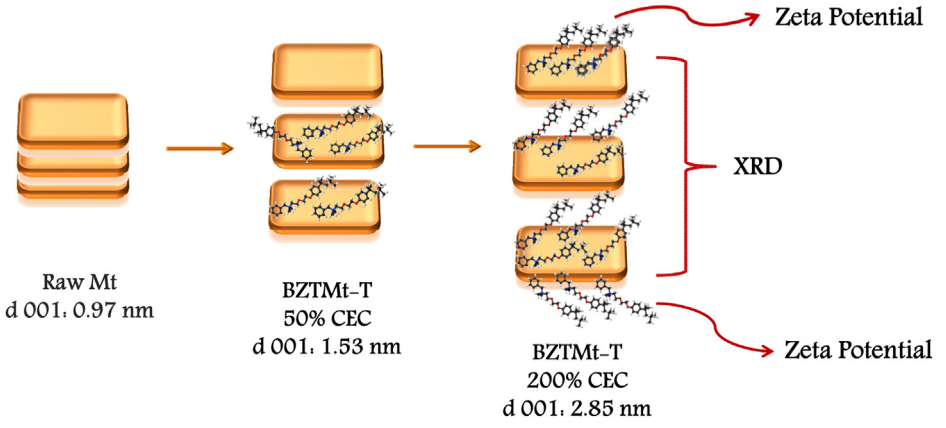

ARTICLE INFO

Article history:
Received 13 December 2016
Received in revised form 1 February 2017
Accepted 6 February 2017
Available online 17 February 2017

Keywords:
Montmorillonite
Benzethonium chloride
Adsorption
Zeta potential
Thermal analysis

ABSTRACT

In this work, Montmorillonite (Mt) obtained from Tokat, Reşadiye region having 0.91 mmol/g cation exchange capacity was modified by using Benzethonium Chloride (BZT). Organoclays, from Mt and BTZ, were prepared by using conventional and microwave heating methods and BTZ in amounts equivalent to 50%, 100% or 200% of CEC of clay. The samples were characterized by XRD, ATR-FTIR, SEM, Thermal analyses and Zeta Potential measurements. Kinetic experiments revealed that adsorption kinetic of BTZ was very fast when the BTZ amount was less than 80% of CEC. The adsorption kinetics fitted to pseudo second order kinetic model for BTZ amounts of 80% and 100% CEC. Adsorption behavior of BTZ on montmorillonite was explained by Sips isotherm model. XRD results indicated that the basal spacing of the clay increased up to 2.85 nm with increasing amount of BTZ and a pseudo trimolecular layer formed in the interlayer. The results of Zeta potential measurements and XRD analyses confirmed the distribution of BTZ between external and internal surfaces.

1. Introduction

Benzethonium Chloride (BZT) is a cationic surfactant with antimicrobial, antiviral, antiseptic properties, and specific activ-

* Corresponding author.
E-mail address: saadetyapar@gmail.com (S. Yapar).

http://dx.doi.org/10.1016/j.colsurfa.2017.02.019
0927-7757/

ity against head and neck cancer [1–3], BZT is used in numerous pharmaceutical formulations as: active ingredient for antiseptics e.g. topical anti-infective in veterinary medicine, [4–7], many fungi and lipid-containing viruses are susceptible to BZT [8] and was also found as efficient non-viral reagent gene vectors due to their safety and other inherent properties over viral delivery techniques to transfect outer DNA into animal cells in vitro [9,10].

Due to its surface activity, BZT can entrap hydrophobic substances within the hydrophobic core or the Stern layer [11]; which enables it as a drug delivery agent by incorporating drugs and biomaterials [8].

The presence of two phenyl rings in the BZT molecule differentiate it from classical detergents where hydrophilic head-group and lipophilic aliphatic chains are clearly separated and hence the aggregation properties of this surfactant is expected to be different from surfactants with aliphatic chains. In this sense recently, Karumbamkandathil et al. [12] indicated that BZT undergoes structural modifications beyond its CMC; changing the BZT micelle from spherical to cylindrical in shape.

Clay minerals, particularly montmorillonite, have been used historically for beneficial healing effects as gastrointestinal and dermatological protectors [13], and some of them have demonstrated antimicrobial and wound healing capabilities [14,15]. Montmorillonite (Mt) is an aluminum silicate composed of hydrated and exchangeable cations sandwiched between the 2:1 (tetrahedral and octahedral) negatively charged layers. It combines high cation exchange capacity and specific surface, as well as good stability in acid media. These properties allowed the classical montmorillonite applications as cationic adsorbent [16], and particularly its selectivity toward ammonium ions and alkyl-ammonium salts make it a material with increasing interest in research for biomedicine [17–22] and to wastewater treatments [23–25]. The ammonium ions or R-ammonium salts selectivity showed by montmorillonite generated the so called organo-montmorillonites, which traditional preparation method for different cationic (ammonium) surfactants used oven heating [24,26–28]. Previous work using microwave in synthesis of silico-aluminate products [29–31] and also in obtaining organo-clays [32] showed that it allows a more direct and rapid heating, reducing the time to a fraction of that generally required using conventional conditions.

In this work, BZT adsorption isotherms on montmorillonite and kinetics data were obtained and thermodynamic parameters were determined. The potential application of BZT-montmorillonite (BZTMt) system as an antiseptic and anti-infective alternative material due to their higher interfacial reactivity, respect to BZT alone, generated the need for understanding the structure of the organo-montmorillonite attained. Two heating methods were used to obtain BZTMt samples: traditional and microwave and some −properties of the products achieved were compared in order to determine the interaction and surface sites involved in the BZT-Mt associations: XRD, FTIR, zeta potential and thermal analysis were used to achieve this objective. Also desorption studies in aqueous media were realized on BZTMt samples obtained by both methods to evaluate the performance of BZT retention.

2. Materials and method

2.1. Materials

A commercial bentonite from Tokat region, central Anatolia of Turkey, provided by Karakaya Bentonite Inc., was purified by sedimentation technique. For this aim, a 10 wt% of montmorillonite-water dispersions were prepared and they were shaken in a water bath at 20 °C for 24 h. After the shaking period, bentonite-water dispersions were diluted to 10% (v/v) and centrifuged to sediment the solid phase according to the Stock Regime 1 min at 2200 rpm. This velocity and time were determined by Stokes Regime to get 2 μm diameter size. The purified Bentonite was labelled Mt. The main properties of Mt, were: cationic exchange capacity (CEC) = 0.91 mmol g^{-1} clay (determined by the Cu-triethylenetetramine method), specific surface area (SSA) = 73 m^2 g^{-1} determined by water vapor adsorption [31], and mineralogical species of raw clay (determined by XRD analysis, using the Rietveld method): Na-montmorillonite (>91%) with Calcite (4.04%) and Cristobalite (4.97%) [30]. The formula of the raw clay was calculated by using the method suggested by Stevens [33] and found as $Na_{0.368}K_{0.032}Ca_{0.059}(Si_{3.8}Al_{0.2})(Al_{1.5}Fe_{0.3}Mg_{0.2})O_{10}(OH)_2n.H_2O$ and by using the XRF results.

The Benzethonium Chloride (BZT) was from Merck KGaA, Germany (≥0.99). The IUPAC name of BZT is, benzyl-dimethyl-[2-[2-[4-(2,4,4-trimethylpentan-2-yl) phenoxy] ethoxy] ethyl] azanium chloride, its molecular weight (MW) = 448.08 g mol^{-1}, Critical Micelle Concentration = 0.56 mM [12] and melting point 158–163 °C [34]. Chloroform, citric acid, disodium hydrogen orthophosphate, and methyl orange were of analytical grade.

2.2. BZT-Mt adsorption experiments

Adsorption experiments were conducted in varying the operating condition of contact time and initial BZT concentration. The adsorption kinetics studies were carried out with a solid/liquid ratio of 0.05 g/50 mL and BZT concentration from 40.7 to 407.7 mg L^{-1}, a time interval from 0 to 1440 min, and at room temperature (20 °C). After the shaking period, each sample was centrifuged at 2500 rpm for 5 min. The supernatants were analyzed following the methyl orange method [35]. Briefly, this method involves mixing methyl orange, citric acid/disodium hydrogen orthophosphate buffer, chloroform and the correspondent supernatant and shaken for 1 min in a separatory funnel. After 20 min, methyl orange allowed to separate the two phases and the underneath part were collected in 100 mL brown colored flask and analyzed by a UV spectrophotometer at λ = 415 nm.

The reversible Pseudo-first-order equation (PFO) equation [36] based on a Lagergren pseudo-first-order rate expression, is described as follows:

$$\ln(Q_e - Q_t) = \ln Q_e - k_1 t \quad (1)$$

Where: k_1 is the pseudo-first-order sorption rate constant, Q_e is the amount of BZT adsorbed at equilibrium by Mt and Q_t is the amount of BZT adsorbed at any time t.

Pseudo-second-order equation (PSO), assumes that the adsorption rate is proportional to the square of the number of unoccupied surface sites. Moreover, the number of occupied sites is proportional to the adsorbate concentration [36]. This model is represented by Eq. (2)

$$\frac{dQ}{dt} = k_2(Q_e - Q_t)^2 \quad (2)$$

Integration of Eq. (2) gives:

$$\frac{t}{Q_t} = \frac{1}{k_2 {Q_e}^2} + \frac{t}{Q_e} \quad (3)$$

Where: k_2 is the PSO adsorption rate constant, $k_2{Q_e}^2$(=H) is the initial sorption rate and Q_e and Q_t are the amount of BZT adsorbed at equilibrium and at a given time, respectively.

The parameters of the equation , k_2 *and* Q_e, were calculated using a linear approach. The adsorption equilibrium study was accomplished with same solid/liquid ratio, within a BZT initial concentration (C_i) from 0 to 407.7 mg L^{-1}, at 20 °C, and pH 5.5 (achieved naturally), and a contact time of 24 h, under shaking (200 rpm) to ensure that the equilibrium was reached in all the adsorption

systems. After the equilibration time the suspensions were centrifuged and filtered. The supernatants were analyzed by using methyl orange method. The amount of adsorbed BZT, *Q*, (mg BZT/g adsorbent) was determined as the difference between the initial BZT concentration (C_i) and that at equilibrium (C_e).

The Langmuir and Sips models, used to adjust the experimental isotherms are given by the Eqs. (4) and (5), respectively.

$$Q_e = \frac{Q_m K_L C_e}{1 + C_e K_L} \quad (4)$$

$$Q_e = \frac{Q_m (K_s C_e)^{\frac{1}{n}}}{1 + (C_e K_s)^{\frac{1}{n}}} \quad (5)$$

In Eq. (4), Q_m is the maximum amount adsorbed within a monolayer ($mg\,g^{-1}$) and k_L ($L\,mg^{-1}$) is the Langmuir dissociation constant, which is related to the adsorption energy. Langmuir isotherm model assumes a monolayer adsorption on a surface with a finite number of identical sites, where all sites are energetically equivalent and without interaction between adsorbed molecules.

In Sips equation (Eq. (5)), K_s ($L\,g^{-1}$) indicates adsorption capacity, and *1/n* (dimensionless) the variation in adsorption as a function of concentration [37].

2.3. Synthesis of organo montmorillonite (BTZ-Mt)

Two heating, traditional and microwave, methods were performed, to attain different BZT loaded Mt samples (BZT-Mt). For both heating methods, 10 g of Mt was added to the solutions containing the BZT equivalent to 50, 100 and 200% CEC value (or 4070 mg L^{-1}, 8140 mg L^{-1},16280 mg L^{-1}) of Mt. Further these dispersions when traditional method was used were stirred for 3 h at 60 °C and 700 rpm, while for microwave method the suspensions were stirred for 5 min at 700 rpm and then subjected 5 min to 360 W of microwave irradiation. For both methods, solid and liquid phases were separated by filtration and solid phase was washed 2 times by 500 mL of distilled water. The collected filtrates were analyzed by methyl orange method to determine the amount of BZT remaining at the end of the adsorption on Mt and/or BZT desorbed during washing. The samples obtained were labelled as BZTMt-YX, were Y indicated the traditional (T) or microwave (M) method and X the BZT loading of the BZTMt as% of CEC value.

2.4. Characterization methods

The structural modifications produced on Mt after the BZT loading were analyzed using the following techniques.

XRD patterns were obtained from power samples using a Philips PW 1710 diffractometer, operated at 40 kV and 30 mA with CuKa radiation. Scans were recorded between 2° and 15° (2θ) with a step size of 0.02° and counting time of 10 s $step^{-1}$.Electrokinetic potentials were determined using Brookhaven 90Plus/Bi-MAS with the electrophoretic mobility function. The electrophoretic mobility was converted into zeta potential values using the Smoluchowski equation. For each determination, 40 mg of sample was dispersed in 40 mL of a 10^{-3} M KCl solution, used as inert electrolyte, and the slurry was stirred. To generate zeta potential versus pH curves, the suspension pH was adjusted using drops of HCl or KOH of different concentrations followed by magnetic stirring until equilibrium was attained (10 min). This equipment allows also determining the particle size by dynamic light scattering (DLS) measurements, using the multiangle particle sizing function. Particle size determinations were performed on a 10^{-3} M KCl solution with a 1% w/w particle dispersion, operating at λ = 635 nm, 15 mW solid state laser, scattering angle = 90°, and temperature = 25 °C. The determination rendered the apparent equivalent sphere diameter, Dapp.

Table 1
Pseudo Second Order (PSO) Kinetic Model Parameters of BZT adsorption on Mt.

Sample	Q_e(mg g^{-1} clay)	k_2(g (mg * h)$^{-1}$)	H(mg (g * h)$^{-1}$)	R^2
BZTMt-T80	320.1 ± 3	0.040 ± 0.05	4123.3	0.999
BZTMt-T100	398.6 ± 8.7	0.012 ± 0.011	1830.3	0.999

Table 2
Parameters of the Langmuir and Sips isotherm models.

Langmuir		Sips	
Q_m ($mg\,g^{-1}$)	372.2± 30	Q_m ($mg\,g^{-1}$)	386.0± 63.7
K_L ($L\,mg^{-1}$)	1.99± 0.698	K_s ($L\,mg^{-1}$)	1.7± 1.132
		1/n	0.89 ± 0.365
R^2	0.987	R^2	0.991

Thermogravimetric (TG) experiments were conducted using a NETZSCH STA 409 PC/PG with alumina as a reference. Samples of 50 mg were placed in Pt crucibles and heated from 30 to 1100 °C at a scanning rate of 10 °C min^{-1} in nitrogen/air atmosphere.

Scanning electron microphotographs of the samples were taken in a JEOL, JFM-6060 scanning electron microscope at different resolutions; 100×, 1000–, 5000× and 10,000×.

ATR-FTIR analyses of the neat BZT, Mt and some BZTMT-T samples were carried out using a Perkin Elmer 100 FTIR spectrometer equipped with an IR source, a KBr beam splitter, and a LiTa03 detector mode and 64 sample and background scans were collected at a resolution of 4 cm^{-1} from 600 to 4000 cm^{-1} in transmittance mode.

2.5. Desorption studies

Desorption experiments were performed, following same procedure used previously [22] on all samples in two steps, adsorption and desorption and all the dispersions containing 0.05 g of montmorillonite and 50 mL of BZT were shaken for 24 h at the adsorption step. At the end of shaking period, one sample was separated to determine the adsorbed amount of BZT and water volume, for testing desorption was added from 50 mL to the 200 mL and the samples were shaken for further 24 h. After the last shaking period, BZT in the supernatants were analyzed using methyl orange method.

3. Results and discussion

3.1. BZT adsorption and desorption studies

The results of kinetic studies showed that the rate of adsorption was very fast for the BZT loading below 80% of CEC and almost all BZT was adsorbed in 15 min. In other words, adsorption kinetic was independent of initial concentration of BZT. However, the time required to reach ~ 100% of adsorption for higher amounts of BZT (>80% CEC) became longer. This behavior was attributed to the steric hindrance of BZT molecules at high concentration. The long alkyl chain of the BZT molecules would probably block both the entrance to the interlayer and also the active sites on the surface at high concentrations.

Pseudo first (PFO) and second order (PSO) kinetic models were used in the evaluation of the data and the PFO Model Parameters determined for samples BZTMt-T80 and BZTMt-T100 gave a $R^2 \leq 0.8$, which indicated a low correlation. The PSO Parameters for both samples were indicated in Table 1.

The obtained isotherms of BZT with the corresponding Sips fit were shown in Fig. 1. The fit correlation coefficients (R^2) and the adjustment parameters obtained from Langmuir and Sips equations are resumed in Table 2. According to the R^2 term, the experimental data were better described by Sips model. Qm cal-

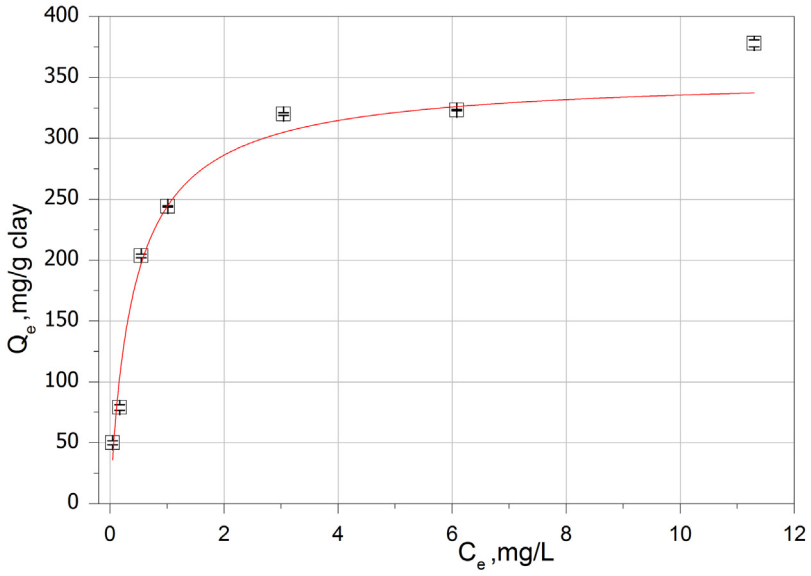

Fig. 1. Adsorption isotherms of BZT on Mt sample. Line indicated: SIPS fit.

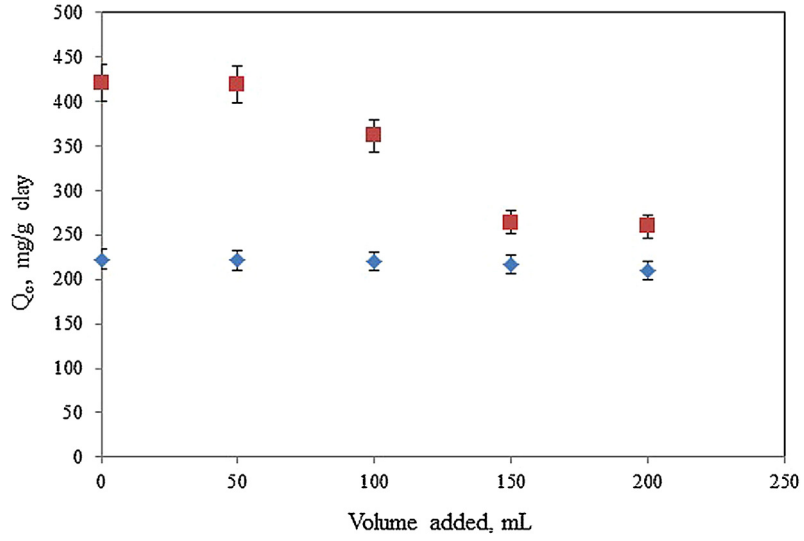

Fig. 2. BZT desorption behavior from Mt samples with *Ci* equivalent to: (◆) 50% and (■) 100% of CEC.

Table 3
BZT remained on clay after washing.

Sample	Amount (%)
BZTMt-M50	99.87 ± 0.96
BZTMt-T50	99.88± 0.96
BZTMt-M100	93.27± 0.96
BZTMt-T100	92.30± 0.96

culated by Langmuir correspond to 91% CEC, and the decrease from 100% CEC was assigned to the steric hindrance of BTZ molecules.

Desorption behavior of BZT for two different initial concentrations (corresponding to 50 and 100% of CEC) was shown in Fig. 2. A higher BTZ desorption was found for BZTMt-T100 than BZTMt-T50 sample. Because the different conditions (temperature, solid liquid ratio, etc.) of the isotherm studies, the amount of surfactant adsorbed in the interlayer and external surfaces and also desorbed during the washing were determined after the organo clay preparation.

Table 3 resumed the percentages of BZT remained on clay with respect to their initial amounts were given.

Although the isotherm studies would indicated the existence of strong interaction between BZT and Mt, as shown Table 3, the increase in the initial amount of BZT causes a decrease in the amount remained in the clay. Both desorption studies and the results obtained from the washing of organoclay indicated that desorption was dependent of the initial concentration and thus of the arrangement of the BZT molecule on the surface. As indicated XRD analyses pseudotrilayer or paraffin-like monomolecular arrangements of BZT was found at higher initial concentrations. Because the interactions between the hydrocarbon tails are not strong enough as in the case of the interactions between clay surface and positively charged head, BZT is desorbed easily at high loadings.

The value of *n* parameter in the Sips equation indicated that the adsorption of the BZT caused the formation of a heterogeneous structure of montmorillonite layers because it was found greater than 1 [38]. Similar behavior was observed by the adsorption of hexadecyltrimethyl-ammonium bromide on same montmoril-

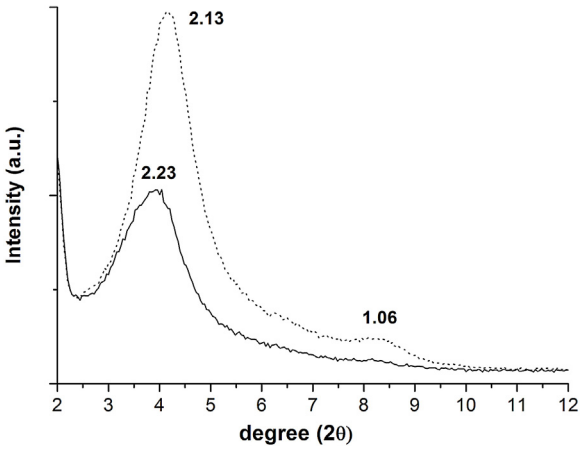

Fig. 3. XRD partial patterns for (dot line) BZTMt-T100 and (full line) BZTMt-M100 samples.

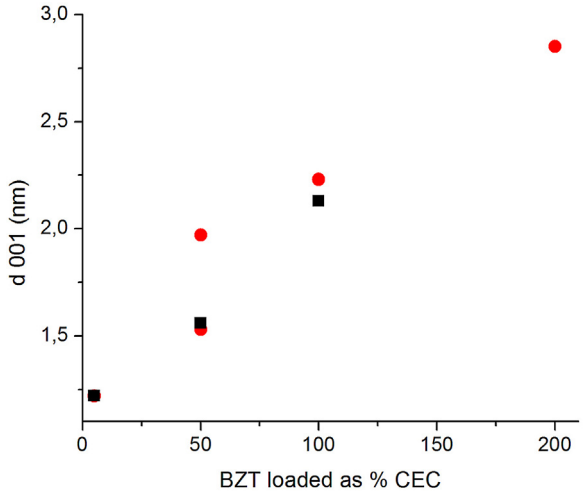

Fig. 4. *d* 001 values against BZTMt loaded samples (Black) BZTMt-T and (●) BZTMt-M samples.

lonite [39]. Yapar and co-workers explained this behavior with the existence of strong chain interactions among the surfactant molecules and these interactions were strong enough to keep HDTMA in the adsorbed layer. The similarity of behavior found for both surfactants would indicate that BZT also have strong enough interactions to stay in the adsorbed layer, and will be discussed in further sections.

3.2. Characterization of BZT loaded Mt obtained by different methods

Mt structural modification after BZT adsorption by traditional and microwave methods was evaluated by XRD, FTIR, zeta potential and TG analysis.

In order to control if the traditional or microwave heating methods performed generated different structure modification XRD partial patterns for BZTMt-T100 and BZTMt-M100 samples were shown in Fig. 3.

The diffractogram of BZTMt-T100 showed the primary reflection at 4.15° 2θ that corresponds to a basal spacing d (001) of 2.13 nm and BZTMt-M100 showed a reflexion at 3.88°2θ (d001 = 2.23 nm). The difference in the basal reflection intensity and width observed between both samples (Fig. 3) and the appearance of a peak at 1.06 nm (or 8.33° 2θ) for BZTMt-T100 sample, could not be assigned to higher order but to multiphase systems involving both regularly and randomly intercalated layers, as was reported for hexadecyltrimethyl-ammonium (HDTMA) surfactant [40,41]. This BZT rearrangement in the Mt interlayer can be involved to the longer time of treatment after traditional than microwave method, which also allowed for BZTMt-T50 sample to develop a second *d* 001 value at 1.97 nm (Fig. S2 in Supplementary material), in agreement to that found by [28] for HDTMA.

The BZT loading in Mt followed through the shift of the Mt basal reflection was shown in Fig. 4, for Mt, BZTMt-T50, BZTMt-M50, BZTMt-T100, BZTMt-M100 and BZTMt-M200 samples.

Classical shifts of the *d* 001 value, towards higher values with BZT loading, for all BZTMt samples respect to that of the Mt sample were observed. The interlayer spaces thicknesses of the BZTMt samples were determined from the difference between the *d*001 value and that of dehydrated Mt (0.97 nm [42]). The calculated interlayer space for BZTMt-T samples were 0.56, 1.25 and 1.88 nm for 50, 100 and 200% CEC exchanged samples respectively, corresponded to a lateral monolayer [43], and pseudotrilayer or paraffin-like monomolecular arrangements of BZT [44], respectively. The last one could come from total remotion of inorganic ions with its hydration sphere partially collapsed layers generated by the surfactant entrance [41,45].

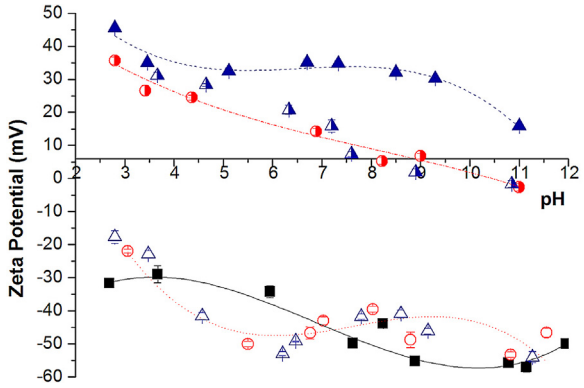

Fig. 5. Zeta potential vs pH curves of all samples. Symbols indicate: (■) Mt; (○) BZTMt-T50; (△) BZTMt-M50; (◑) BZTMt-T100; (◭) BZTMt-M100 and (▲) BZTMt-M200 samples.

Fig. 5 showed zeta potential vs pH curves for Mt and BZTMt-T and BZTMt-M samples. The Mt sample showed the classical zeta potential behavior pH-independent (at around −30 mV) over a wide pH range (from pH 2–12) [46–48]. No significant differences between zeta potential curves of the BZTMt-T50 and BZTMt-M50 samples and that of Mt sample were observed. In contrast, a reversal surface electric charge was found for samples with BZT loaded with 100% CEC (BZTMt-M100 and BZTMt-T100 samples) respect to that observed for Mt sample. The positive surface electric charge found for BZTMt-M100 and BZTMt-T100 samples, with surfactant loading close to the CEC, was assigned to surfactant coverage of external surface in bilayer arrangements [49], Mt structural charges were neutralized at loading of different cationic dyes very close to the CEC [50] generating an isoelectric point at pH = 8.5. The further loading of cationic BZT (BZTMt-M200 sample) were governed by the charging behavior of the edge surfaces of the particles with some positive ammonium groups oriented out of the surface [41].

These electric charge changes contributed to originate a 10 times aggregates enlargement (from 680 to around 7000 nm, measured as apparent diameter, at pH = 5.5, Table S1 in Supplementary material) of OMt (with 50 and 100 CEC loading) respect to Mt samples in agreement with data found by Gamba et al. [24]. Particularly, for BZTMt-M200 sample the reversal to higher positive charge respect

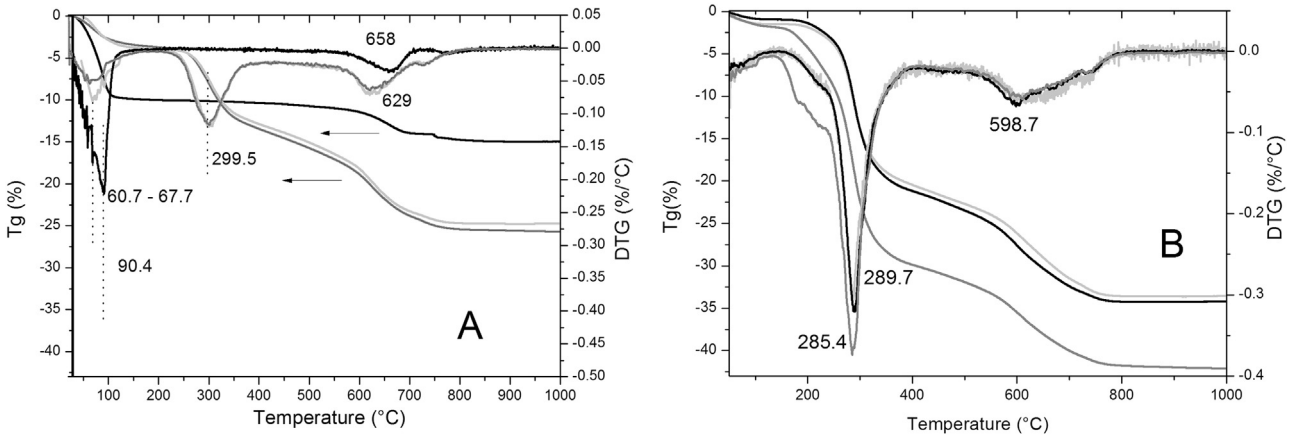

Fig. 6. DTG and TG curves of: (A) (black line) Mt, (dark grey line) BZTMt-T50 and (grey line) BZTMt-M50 and (B) (black line) BZTMt-T100, (grey line) BZTMt-M100 and (dark grey line) BZTMt-M200 samples.

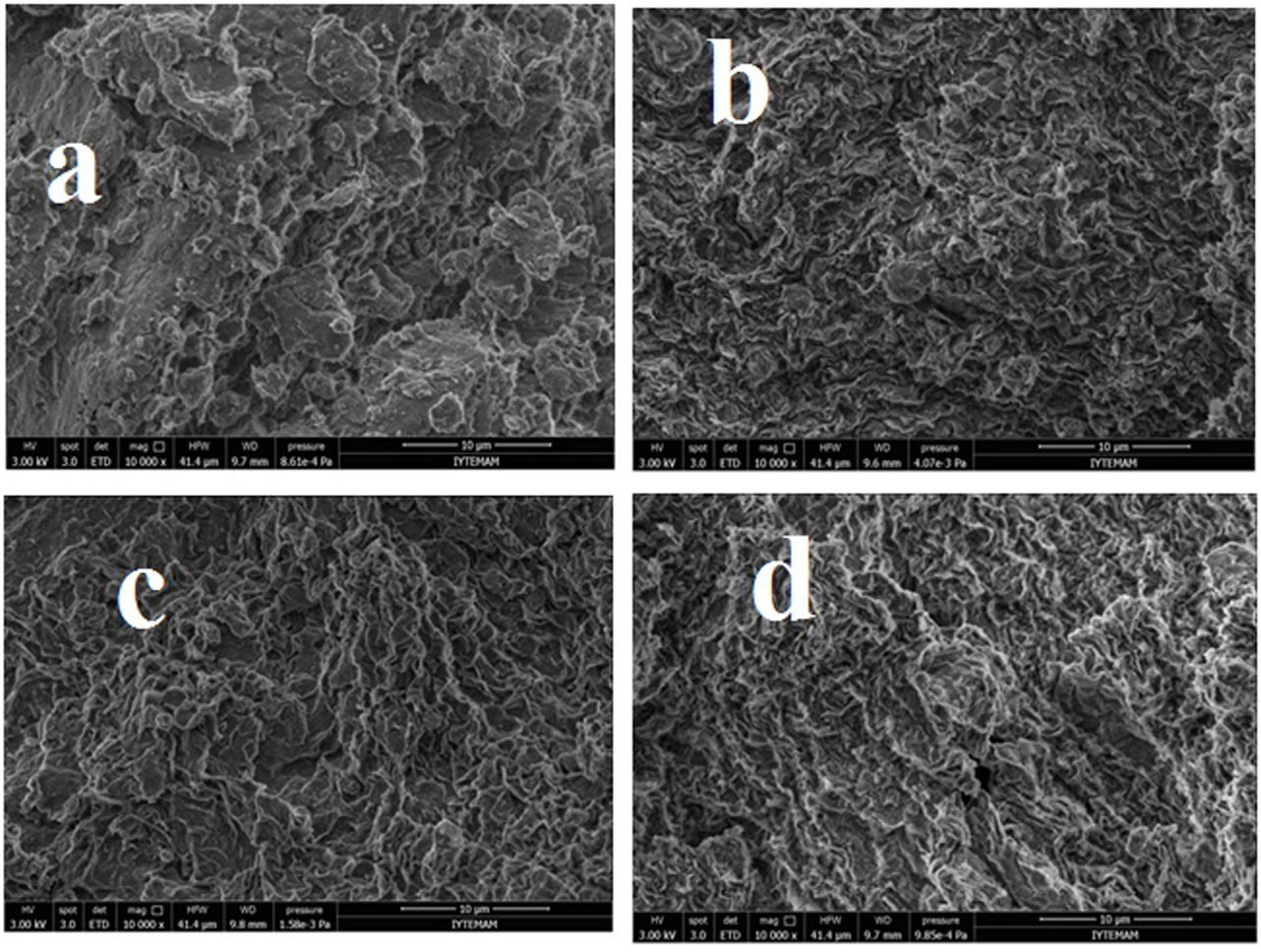

Fig. 7. SEM for (A) Mt; (B) BZTMt-M50; (C) BZTMt-M100 and (D) BZTMt-M200 samples.

to BZTMt-M100 generated a Dapp decrease from 7000 to 1718 nm (Table S1 in Supplementary material).

TG analyses (Fig. 6A and B) indicated several mass-loss steps, particularly the mass loss before 200 °C was attributed to the dehydration of physically adsorbed water and water molecules around metal cations on exchangeable sites in Mt [51]. The water content in BZTMt samples were lower than in Mt (22.5%, Fig. 6A and B) and decreased from BZTMt-T50 to BZTMt-T100, due to the increasing hydrophobicity of the samples.

The mass loss occurring from 200 °C to 300 °C was attributed to the decomposition of the BZT (Fig. S3 in Supplementary material). The de-surfactant temperature, obtained from derivative-Tg (DTg) curves, decreased from 299.5 °C for BZTMt-T50 and BZTMt-M50 samples with BZT loading attaining 285.4 °C for BZTMt-M200 sample, in agreement to the thermal stability of organoclays

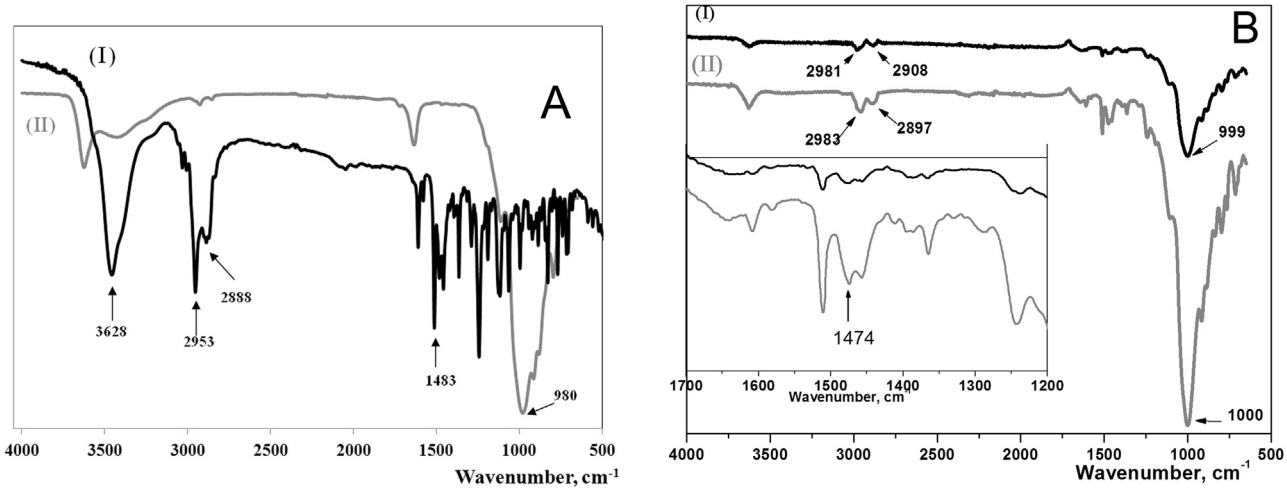

Fig. 8. Figure 8. ATR-FTIR spectra of: (A) (black line, I) neat BZT and (grey line, II) Mt sample and (B) (black line, I) BZTMt-T50 and (grey line,II) BZTMt-T100 samples.

Table 4
Calculated BZT loading in the obtained organoclays.

Sample	S (%)	BZT loaded value respect CEC (with Cl^-)	BZT loaded value respect CEC (without Cl^-)
BZTMt-M50	16.23	47.5	57.8
BZTMt-T50	17.32	51.4	62.6
BZTMt-M100	28.1	95.9	116.7
BZTMt-T100	26.51	88.5	107.7
BZTMt-M200	32.75	119.5	145.4

decrease with loading surfactant increase suggested previously [52,53]. Finally, the mass-loss over the temperature from 500 to 800 °C was ascribed to the loss of the structural OH units of the montmorillonite [54]. The temperature decrease of this peak with surfactant loading increased in agreement to that found by [53] for octadecyltrimethyl-Mt samples was assigned to charcoal oxidation (high temperature stable charcoal) which occurs simultaneously with the dehydroxylation of the clay and its transformation into amorphous meta-MONT [55].

From the TG results the real amounts of BZT in BZTMt samples were calculated based on the data for the second mass-loss region following the eq. 6 indicated in Sun et al. [56] and the calculated results are summarized in Table 4.

$$L = \frac{S10^5}{(MW - y)(100 - S)CEC} \quad (6)$$

where L is the calculated loaded BZT amount; MW is the BZT molecular weight; S is the mass loss percentage of BZT in BZTMt sample; y is 0 (if all the Cl^- remain) or 35.5 (no Cl^-; MW of Cl^- = 35.5).

Table 4 indicated that the amount of BZT loaded in the BZTMt is close to that predicted by the theoretical values in each sample if all the Cl^- was eliminated by washing, in agreement with the charge reversion found by zeta potential measurements, and also with that found by Pecini and Avena [50] for didodecyldimethylammonium bromide loaded Mt. The low value of BZT loading (Table 4) calculated for BZTMt-M200 sample would be originated by micelles formation due to the high BZT concentration used and further elimination by washing.

The SEM image of Mt sample (Fig. 7a) revealed traditional face-to-edge contact between the particles with random orientation, and some agglomerates were identified. The BZT loading increases in BZTMt-M50, BZTMt-M100 and BZTMt-M200 samples (Fig. 7b–d, respectively) indicate a curly character increase with the BZT loading in agree with behavior found by Lee and Kim [57] for HDTMA loaded montmorillonite with 2.5 times the respective CEC.

The ATR-FTIR spectroscopy from 450 to 4000 cm^{-1} provided information about the structural changes that occurred after BZT adsorption and allows identifying groups association with the solid surface (Fig. 8A and B). To identify the characteristic bands of BZT the spectra of cationic surfactant were measured and that of Mt were added (Fig. 8A). As shown in Fig. 8A, typical bands of crude montmorillonite at 3628, 1635 and 980 cm^{-1} assigned to OH stretching, to OH deformation and to Si-O stretching, respectively, were observed. In the spectrum of BZT characteristic bands were appeared at 2953, 2888 and 1483 cm^{-1} were assigned to asymmetric CH_2 stretching, symmetric CH_2 stretching and CH_2 scissors, respectively [58,59].

Fig. 8B displays the typical spectra of BZTMt-T samples at two percentage of CEC (50 and 100%). The bands originating from BZT were observed at higher or lower frequencies depending on surfactant loading (Table S2 in Supplementary material). The shifts observed in the bands were indication of conformational changes, intermolecular interactions between the chains and also with the siloxane surface [58,60].

The peaks at 2953 cm^{-1} and 2888 cm^{-1} for neat BZT (Fig. 8A) shifted to higher wavenumbers in organoclays except for BZTMt-T100 sample (Fig. 8B) pointing out the interactions between BZT and clay surface. The peak assigned to Si-O stretching at 980 cm^{-1} for Mt sample (Fig. 8A) shifted to higher wavenumbers, 999, 1000 and 995 cm^{-1} for BZTMt-T50, BZTMt-T100 and BZTMt-T200 samples (Fig. 8 B), respectively. This peak shifts correspond to the interaction of BZT with siloxane surface and the intensity increase was indicative of the BZT loading increase and interlayer replacement of small Na^+ by BZT cations [59]. Additionally, CH_2 scissors band of neat BZT at 1483 cm^{-1} shifted to 1474 cm^{-1} when loaded in the respective BZTMt samples. The presence of a peak at 1474 cm^{-1} and it increase with the BZT loading in the respective BZTMt samples showed the methylene chains ordered in *all-trans* crystalline state [58].

4. Conclusion

Although BZT has a high molecular size, it has rapid adsorption kinetics especially at low concentrations. The adsorption rate decreases with increasing BZT concentration found was attributed to a steric hindrance. A maximum adsorption capacity of 386.0 mg/g was found using Sips mathematical model.

No evidence of changes in the arrangements of BZT, generated by the two intercalation methods studied, were found by XRD analysis, however a multiphase systems involving both regularly and randomly intercalated layers seems to be attained by traditional method. External Mt surface was involved in the BZT adsorption when the amount exchanged attained the CEC value. FTIR analyses indicated that BZT directly interact with the siloxane surface of the Mt.

Desorption studies revealed that the initial amount of BZT and volume of water added (dilution) were of importance. Desorbed amounts increased with initial amount of BZT and also the water volume of washed.

These results promote the potential application of BZT-Mt as alternative disinfectants because its immobilized form would be less irritant and long lasting.

Acknowledgements

We sincerely thank financial support of Argentine Ministry of Science, Technology and Productive Innovation – ANPCyT- PICT 2014/585. R.M.T.S. is member of CONICET and F.Y. acknowledged CONICET fellowship.

Appendix A. Supplementary data

Supplementary data associated with this article can be found, in the online version, at http://dx.doi.org/10.1016/j.colsurfa.2017.02.019.

References

[1] F.M. Menger, The structure of micelles, Acc. Chem. Res. 12 (4) (1979) 111–117.
[2] H.H. Paradies, U. Hinze, M. Thies, Hydrodynamic studies on benzethonium chloride micelles in dilute aqueous solution, Ber. Bunsen-Ges. Phys. Chem. 98 (7) (1994) 938–946.
[3] H.H. Paradies, H. Reichelt, Influence of the anions on the N-cationic benzethonium salts in the solid state and solution: chloride bromide, hydroxide and citrate hydrates, AIP Adv. 6 (6) (2016) 065322.
[4] H.A. Bruson, U.S. patent 2, 115,250A, 1938.
[5] F. Coulston, H.P. Drobeck, Z.E. Mielens, P.J. Garvin, Toxicol. Appl. Pharm. 3 (6) (1961) 584–594.
[6] The Merck Index, 13th edition, # 1074, Merck & Co, Inc., Whitehouse Station, New Jersey, 2001.
[7] A. Goodman Gilman, L.S. Goodman, T. Rall, F. Murad, Goodman and Gilman's The Pharmacological Basis of Therapeutics, 7th ed., MacMillan Publisher Company, N. Y, 1985, pp. 950–971.
[8] H. Paradies, US-Patent 4074850 (1989).
[9] J.K. Rose, U.S. patent 5,279,833 (1994).
[10] E. Lee, C. Oh, I.S. Kwon, I.C. Kwon, S. Kim, Co-delivery of chemosensitizing siRNA and an anticancer agent via multiple monocomplexation-induced hydrophobic association, J. Controlled Release 210 (2015) 105–114.
[11] D. Attwood, A.T. Florence, Reactivity in surfactant systems, in: D. Attwood (Ed.), Surfactant Systems, Springer, Netherlands, 1983, pp. 698–777 (ISBN 978-94-009-5775-6).
[12] A. Karumbamkandathil, S. Ghosh, U. Anand, P. Saha, M. Mukherjee, S. Mukherjee, Micelles of benzethonium chloride undergoes spherical to cylindrical shape transformation: an intrinsic fluorescence and calorimetric approach, Chem. Phys. Lett. 593 (2014) 115–121.
[13] M.I. Carretero, M. Pozo, Clay and non-clay minerals in the pharmaceutical and cosmetic industries Part II. Active ingredients, Appl. Clay Sci. 47 (3–4) (2010) 171–181.
[14] L.B. Williams, M. Holland, D.D. Eberl, T. Brunet, L.B. De Courrsou, Killer clays! Natural antibacterial clay minerals, Mineral. Soc. Bull. 139 (2004) 3–8.
[15] E.E. Gaskell, A.R. Hamilton, Antimicrobial clay-based materials for wound care, Future Med. Chem. 6 (6) (2014) 641–655.
[16] S.M. Magaña, P. Quintana, D.H. Aguilar, J.A. Toledo, C. Angeles- Chavez, M.A. Cortez, L. León, Y. Freile-Pelegrin, T. López, R.M. Torres Sánchez, Antibacterial activity of montmorillonites modified with silver, J. Mol. Catal. A 281 (2008) 192–199.
[17] P. Herrera, R.C. Burghardt, T.D. Phillp, Adsorption of salmonella enteritidis by cetylpyridinium- exchanged montmorillonite clays, Vet. Microbiol. 74 (2000) 259–272.
[18] A. Magnoli, L. Tallone, C. Rosa, A.M. Dalcero, S.M. Chiacchiera, R.M. Torres Sánchez, Commercial bentonites as detoxifier as broiler feed contaminated with aflatoxins, Appl. Clay Sci. 40 (2008) 63–71.
[19] N. Meng, N.L. Zhou, S.Q. Zhang, J. Shen, Synthesis and antimicrobial activities of polymer/montmorillonite–chlorhexidine acetate nanocomposite films, Appl. Clay Sci. 42 (3) (2009) 667–670.
[20] S. Mishra, P.L. Nayak, B.C. Guru, P.K. Nanda, Synthesis and characterization of poly urethane nanocomposites for biomedical applications, Bioscan 2 (2010) 403–412.
[21] G. Özdemir, M. Hosgör Limoncu, S. Yapar, Antibacterial effect of heavy metal and cetylpyridinium exchanged montmorillonites, Appl. Clay Sci. 48 (2010) 319–323.
[22] G. Özdemir, S. Yapar, H. Limoncu, Preparation of cetylpyridinium montmorillonite for antibacterial applications, Appl. Clay Sci. 72 (2013) 201–205.
[23] S.M. Lee, D. Tiwari, Organo and inorgano-organo-modified clays in the remediation of aqueous solutions: an overview, Appl. Clay Sci. 59 (2012) 84–102.
[24] M. Gamba, F.M. Flores, J. Madejová, R.M. Torres Sánchez, Comparison of imazalil removal onto montmorillonite and nanomontmorillonite and adsorption surface sites involved: an approach for agricultural wastewater treatment some aspects of the adsorption of the fungicide imazalil onto octadecyltrimethylammonium, Ind. Eng. Chem. Res. 54 (2015) 1529–1538.
[25] L. Zhang, B. Zhang, T. Wu, D. Sun, Y. Li, Adsorption behavior and mechanism of chlorophenols onto organoclays in aqueous solution, Colloids Surf. A 484 (2015) 118–129.
[26] B. Zidelkheir, M. Abdelgoad, Effect of surfactant agent upon the structure of montmorillonite, J. Therm. Anal. Calorim. 94 (1) (2008) 181–187.
[27] H. He, Y. Ma, J. Zhu, P. Yuan, Y. Qing, Organoclays prepared from montmorillonites with different cation exchange capacity and surfactant configuration, Appl. Clay Sci. 48 (2010) 67–72.
[28] J. Zhu, T. Wang, R. Zhu, F. Ge, P. Yuan, H. He, Expansion characteristics of organo montmorillonites during the intercalation, aging, drying and rehydration processes: effect of surfactant/CEC ratio, Colloids Surf. A 384 (2011) 401–407.
[29] S.-E. Park, D.S. Kim, J.-S. Chang, W.Y. Kim, Synthesis of MCM-41 using microwave heating with ethylene glycol, Catal. Today 44 (1998) 301–308.
[30] M. Emreol, N. Soycan, S. Yapar, Adsorption properties of microwave synthesized inorgano-organo montmorillonite, Asia-Pac. J. Chem. Eng. 5 (2010) 369–377.
[31] S. Yapar, Physicochemical study of microwave-synthesized organoclays, Colloids Surf. A 345 (2009) 75–81.
[32] S. Yapar, R.M. Torres Sanchez, M. Emreol, P. Weidler, K. Emmerich, Microwave irradiation used for all steps of pre-pillaring Al-montmorillonite, Clay Miner. 44 (2009) 267–278.
[33] R. Stevens, A system for calculating analyses of micas and related minerals to end members, US Geol. Surv. Bull. 950 (1945) 101–119.
[34] The Merck Index – Encyclopedia of Chemicals, Drugs and Biologicals, in: S. Budavari (Ed.), Merck and Co., Inc., Rahway, NJ, 1989, p. 167.
[35] L.K. Wang, D.F. Langley, Determining cationic surfactant concentration, Ind. Eng. Chem. Prod. Res. Dev. 14 (3) (1975) 210–212.
[36] A.K. Bhattacharya, C. Venkobachar, Removal of cadmium (II) by low cost adsor-bents, J. Environ. Eng. 110 (1984) 110–122.
[37] M.J. Sanchez-Martin, M.S. Rodriguez-Cruz, M.S. Andrades, M. Sanchez-Camazano, Efficiency of different clay minerals modified with a cationic surfactant in the adsorption of pesticides: influence of clay type and pesticide hydrophobicity, Appl. Clay Sci. 31 (3–4) (2006) 216–228.
[38] S. Tedds, A. Walton, D.P. Broom, D. Book, Characterisation of porous hydrogen storage materials: carbons, zeolites, MOFs and PIMs, Faraday Discuss. 151 (2011) 75–94.
[39] S. Yapar, V. Özbudak, A. Dias, A. Lopes, Effect of adsorbent concentration to the adsorption of phenol on hexadecyl trimethyl ammonium-bentonite, J. Hazard. Mater. B121 (2005) 135–139.
[40] H. He, R.L. Frost, T. Bostrom, P. Yuan, L. Duong, D. Yang, Y. Xi, J.T. Kloprogge, Changes in the morphology of organoclays with HDTMA+ surfactant loading, Appl. Clay Sci. 31 (2006) 262–271.
[41] A.E. Bianchi, M. Fernández, M. Pantanetti, R. Viña, I. Torriani, R.M. Torres Sánchez, G. Punte, ODTMA$^+$ and HDTMA$^+$ organo-montmorillonites characterization: new insight by WAXS SAXS and surface charge, Appl. Clay Sci. 83–84 (2013) 280–285.
[42] K. Emmerich, M. Plötzeand, G. Kahr, Reversible collapse and Mg2+ release of de- and rehydroxylated homoionic cis-vacant montmorillonites, Appl. Clay Sci. 19 (1–6) (2001) 143–154.
[43] G.W. Brindley, W.F. Moll, Complexes of natural and synthetic Ca-montmorillonites with fatty acids, Am. Mineral. 50 (1965) 1355–1370.
[44] J. Zhu, H. He, J. Guo, D. Yang, X. Xie, Arrangement models of alkylammonium cations in the interlayer of HDTMA + pillared montmorillonites, Chin. Sci. Bull. 48 (4) (2003) 368–372.
[45] S. Baldassari, S. Komarneni, E. Mariani, C. Villa, Microwave versus conventional preparation of organoclays from natural and synthetic clays, Appl. Clay Sci. 31 (1–2) (2006) 134–141.
[46] S.E. Miller, P.F. Low, Characterization of the electrical double layer of montmorillonite, Langmuir 6 (3) (1990) 572–578.
[47] F. Thomas, L.J. Michot, D. Vantelon, E. Montargès, B. Prélot, M. Cruchaudet, J.F. Delon, Layer charge and electrophoretic mobility of smectites, Colloids Surf. A 159 (2–3) (1999) 351–358.
[48] B.M. Lombardi, R.M. Torres Sanchez, P. Eloy, M. Genet, Interaction of thiabendazole and benzimidazole with montmorillonite, Appl. Clay Sci. 33 (1) (2006) 59–65.

[49] P. Praus, M. Turicová, S. Študentová, M. Ritz, Study of cetyltrimethylammonium and cetylpyridinium adsorption on montmorillonite, J. Colloid Interface Sci. 304 (1) (2006) 29–36.
[50] E.M. Pecini, M.J. Avena, Measuring the isoelectric point of the edges of clay mineral particles: the case of montmorillonite, Langmuir 29 (2013) 14926–14934.
[51] Y. Li, H. Ishida, Concentration-dependent conformation of alkyl tail in the nanoconfined space: hexadecylamine in the silicate galleries, Langmuir 19 (6) (2003) 2479–2484.
[52] A. Vazquez, M. López, G. Kortaberria, L. Martín, I. Mondragon, Modification of montmorillonite with cationic surfactants. Thermal and chemical analysis including CEC determination, Appl. Clay Sci. 41 (1–2) (2008) 24–36.
[53] Y. Xi, W. Martens, H. He, R.L. Frost, Thermogravimetric analysis of organoclays intercalated with the surfactant octadecyltrimethylammonium bromide, J. Therm. Analysis Calorim. 81 (2005) 91–97.
[54] J.L. Bishop, C.M. Pietersand, J.O. Edwards, Infrared spectroscopic analyses on the nature of water in montmorillonite, Clays Clay Miner. 42 (6) (1994) 702–716.
[55] S. Yariv, I. Lapides, M. Borisover, Thermal analysis of tetraethylammonium and benzyltrimethylammonium montmorillonites, J. Therm Anal. Calorim. 110 (2012) 385–394.
[56] Z. Sun, Y. Park, S. Zheng, G.A. Ayoko, R.L. Frost, XRD TEM, and thermal analysis of Arizona Ca-montmorillonites modified with didodecyldimethylammonium bromide, J. Colloid Interface Sci. 408 (2013) 75–81.
[57] S.Y. Lee, S.J. Kim, Expansion characteristics of organoclay as a precursor to nanocomposites, Colloids Surf. A 211 (2002) 19–26.
[58] R.A. Vaia, R.K. Teukolsky, E.P. Giannelis, Interlayer structure and molecular environment of alkylammonium layered silicates, Chem. Mater. 6 (1994) 1017–1022.
[59] M. Majdan, O. Maryuk, A. Gładysz-Płaska, S. Pikus, R. Kwiatkowski, Spectral characteristics of the bentonite loaded with benzyldimethyloctadecylammonium chloride, hexadecyltrimethylammonium bromide and dimethyldioctadecylammonium bromide, J. Mol. Struct. 874 (2008) 101–107.
[60] N. Banik, S.A. Jahan, S. Mostofa, H. Kabir, N. Sharmin, M. Rahman, S. Ahmed, Synthesis and characterization of organoclay modified with cetylpyridinium chloride, Bangladesh, J. Sci. Ind. Res. 50 (1) (2015) 65–70.